J. Eur. Opt. Society-Rapid Publ. 2024, **20**, 7

https://doi.org/10.1051/jeos/2024006
Available online at: https://jeos.edpsciences.org

Journal of the European Optical Society-Rapid Publications

EOSAM 2023
Guest editors: Patricia Segonds, Guy Millot and Bertrand Kibler

RESEARCH ARTICLE OPEN ACCESS

µJ-level normal-dispersion fiber optical chirped-pulse parametric oscillator

Tristan Guezennec[1,2], Saïd Idlahcen[1], Armand Cervera[1], Pierre-Henry Hanzard[1], David Landais[2,a], Laurent Provino[2], Adil Haboucha[2], Thomas Godin[1,*], and Ammar Hideur[1]

[1] CORIA, UMR 6614 CNRS – INSA Rouen – Université de Rouen Normandie, 675 avenue de l'Université, 76801 Saint Etienne du Rouvray, France
[2] Photonics Bretagne, 4 rue Louis de Broglie, 22300 Lannion, France

Received 30 January 2024 / Accepted 16 February 2024

Abstract. We demonstrate the generation of broadband tunable and synchronized pulses exceeding the microjoule level using the new concept of Fiber Optical Parametric Chirped-Pulse Oscillation (FOPCPO). The oscillator is based on a collapsed-ends photonic crystal fiber pumped in the normal dispersion regime by an ytterbium fiber laser delivering highly-chirped pulses. The experimental results are compared with the results of numerical simulations and highlight that the feedback ratio appears as a key parameter for optimizing the system's efficiency and dynamics.

Keywords: Parametric Sources, Nonlinear Fibers, Fiber laser, Ultrafast laser, Parametric oscillator, FOPCPO.

1 Introduction

Optical parametric amplifiers and oscillators delivering ultrashort pulses are a well-established technology that has enabled considerable progresses in many research and industrial applications [1]. Multi-mJ energies and few cycles pulse durations are now reached using solid-state optical parametric sources but their complexity, cost, and alignment sensitivity hinder their use outside the laboratory environment. In the last years, significant advances have been made in their fiber-based counterparts which rely on Degenerate Four-Wave Mixing (DFWM – third-order nonlinearity of silica). Nonlinear wavelength conversion of ultrashort pulses has then been obtained with a variety of fiber systems. In particular, using the concept of Fiber Optical Parametric Chirped-Pulse Amplification (FOPCPA) [2–4] has allowed to overcome the saturation of the nonlinear process and the µJ level has been reached, by either using complex optical fiber designs or using Raman gain assistance. However, such systems operate in the anomalous group velocity dispersion of the fiber which restricts the parametric sidebands near the pump wavelength. FOPCPA pumped in the normal dispersion regime and delivering sub-picosecond pulse with wide wavelength separations have been reported but are still limited in terms of tunability as they require a seed source [5–7]. A way to circumvent this limitation is to use a resonant fiber optical parametric oscillator (FOPO) where the dispersion map can be tailored. High energy levels and ultrashort pulses – along with excellent signal-to-noise ratios – have then been obtained in FOPOs combining DFWM in Photonic Crystal Fibers (PCF) with pumping in the normal dispersion regime [8, 9]. Further energy scaling is however quite limited due to high peak powers and subsequent nonlinearities. To overcome this limitation, a natural idea is then to combine FOPCPAs capabilities in terms of energy scaling by using chirped pulses with FOPO's flexibility and wavelength tunability. Such a concept – termed FOPCPO – was first investigated numerically and showed significant potential for bandwidth control of parametric waves [10]. We then demonstrated experimentally the feasibility of this concept by generating broadly-tunable highly chirped pulses with energies exceeding 200 nJ in such a FOPCPO [11]. By combining highly-chirped pump pulses with a collapsed-ends photonic crystal fiber, we now confirm this idea and report on the generation of broadband signal and idler waves exceeding the µJ level at MHz-repetition rates from a FOPCPO pumped in the normal dispersion regime.

2 Experimental set-up

The experimental setup is depicted in Figure 1. The pump laser is a commercial ytterbium fiber laser (*Active Fiber Systems GmbH*), delivering highly-chirped pulses of 800 ps at 1032 nm (200 fs transform-limited) with 15 W average

[a] Currently at Lumibird, Lannion, France
* Corresponding author: thomas.godin@coria.fr

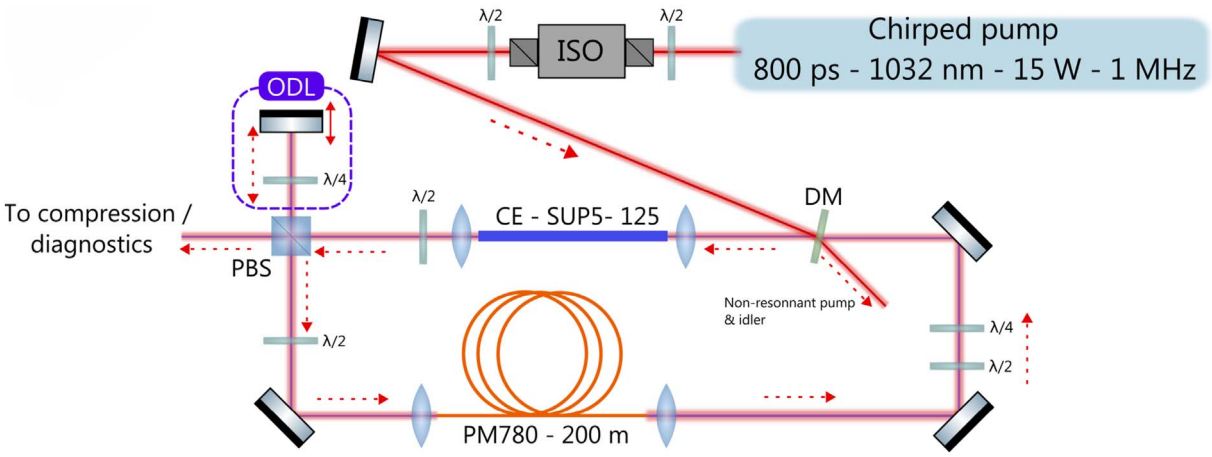

Figure 1. Experimental setup. ISO: Isolator, CE-SUP5-125: Collapsed-ends SUP5-125 fiber, DM: Dichroic mirror, PBS: Polarization beam splitter, ODL: Optical delay line.

power at 1 MHz repetition rate. The pump pulses are injected into the nonlinear fiber through a combination of a dichroic mirror and an aspheric lens (11 mm focal length).

The nonlinear fiber is an air-silica micro-structured 8 cm long SUP-5-125 (Product line Perfos®) fiber, developed and drawn at Photonics Bretagne facilities. It exhibits a nonlinear coefficient of 15 $W^{-1}{\cdot}m^{-1}$, a 5 µm mode field diameter, and a zero-dispersion wavelength of 1055 nm. Both ends of the fiber are collapsed in order to mitigate the laser induced damages due to the high peak power coming from the pump laser (up to 20 kW). The collapsed region is tailored to avoid beam diffraction on the fiber tip, resulting in an excellent output beam quality, as shown in Figure 2c on the beam profile taken at directly at the output of the fiber. As the phase-matching diagram depicted in Figure 2a suggest, such a fiber should generates a signal wave in the 800 nm band, along with an idler wave in the 1500 nm band.

The cavity is closed with a 200 m PM780 spool, so the signal wave propagates in the normal dispersion regime allalong the intracavity components, and match the repetition rate of the pump laser. In order to finely adjust the roundtrip delay of the cavity, we also implemented an Optical Delay Line (ODL), which allows us to tune the emission wavelength using a dispersive filtering effect [12]. This indeed gives the possibility to overlap different spectral components of the pump pulses and the signal pulses, hence changing the phase-matching condition of the parametric process. The feedback ratio is controlled via an adjustable optical circulator before the ODL, and the polarization of the signal is controlled in the cavity in order to improve the parametric conversion and to mitigate any polarization-dependent phase mismatching in the nonlinear fiber.

3 Numerical simulations

3.1 Numerical FOPCPO model

In order to predict the FOPCPO performances, we developed a script for a typical cavity as depicted in Figure 3. The script propagates the complex optical envelop through the different fibers and components, and reuse a fraction of the output field into the next cavity roundtrip. Numerical simulations along the fiber segments were performed using an in-house Generalized Nonlinear Schrödinger Equation (GNLSE) solver, with a Runge-Kutta 4 in Interaction Picture (RK4IP) method [13]. The main idea is to solve the following GNLSE:

$$\frac{\partial A(z,T)}{\partial z} = \underbrace{-\frac{\alpha(\omega)}{2}A(z,T) + \sum_{k\geq 2}\frac{i^{k+1}}{k!}\beta_k\frac{\partial^k A(z,T)}{\partial T^k} + \ldots}_{\hat{L}} \underbrace{\ldots i\gamma\left(1+\tau_{\text{shock}}\frac{\partial}{\partial T}\right)\times\left(A(z,T)\int_{-\infty}^{\infty}R(T')|A(z,T-T')|^2\mathrm{d}T'\right)}_{\hat{N}} \tag{1}$$

By applying the following transformation,

$$A_I(z,T) = e^{(z-z')\hat{L}}A(z,T) \tag{2}$$

it is possible to solve equation (1) using standard Runge-Kutta 4 algorithm. The fibers parameters (*i.e.* the Taylor coefficients β_k and the nonlinear coefficient γ) were determined using an in-house developed fiber mode solver based on a finite- difference method, while the material loss α are approximated using the fused silica losses model presented in [14]. The pump pulses are modeled using:

$$A(t) = \sqrt{P_0}e^{-1/2\left(\frac{t-\tau}{t_0}\right)^2}e^{i\left(\frac{C_2}{2}(\omega-\omega_0)^2\right)-i\omega_0 t} \tag{3}$$

where C_2 is the 2nd order phase coefficient that control the quadratic phase (i.e. the chirp) of the pulse [15]. In order to initiate the parametric fluorescence in the nonlinear fiber, the pump pulses are injected with a noise of one photon per spectral mode.

The numerical parameters used in the simulations are detailed in Table 1.

The pump pulses are defined as linearly chirped gaussian pulse, with a Fourier-limited duration of 200 fs, energies of

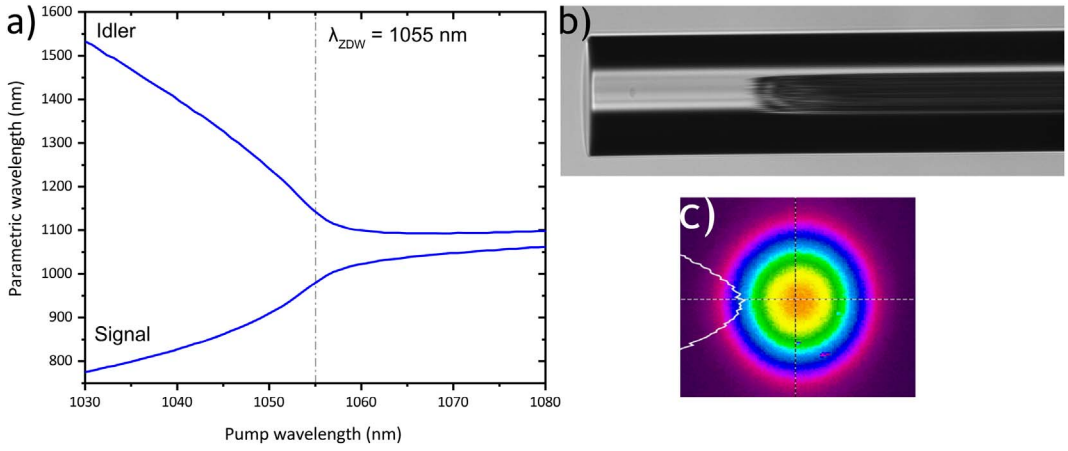

Figure 2. a) Phase matching diagram of the SUP5-125 fiber. b) Collapsed-end of the SUP5-125 fiber. c) Beam profile at the output of the SUP5-125 fiber

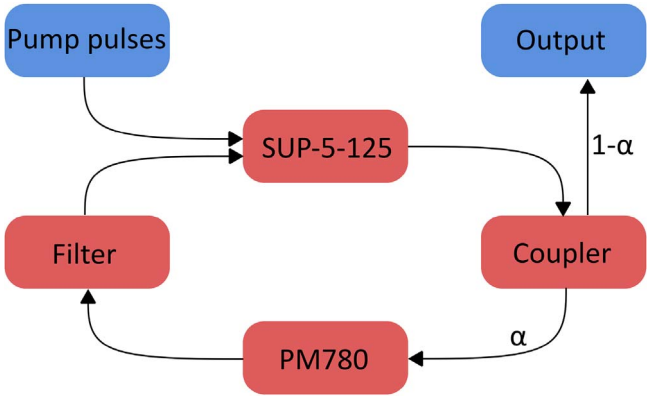

Figure 3. Outline of the cavity simulation.

10 µJ, and a 2nd order phase coefficient of $5.8 \cdot 10^{-23}$ s^2, leading to a pulse duration of 800 ps at 1032 nm.

3.2 Numerical results

Simulations were performed for 100 roundtrips in the cavity. As depicted in Figure 4, we extracted narrowband signal pulses of 1.2 µJ centered at 785 nm, along with broadband idler pulses of 650 nJ, exceeding our previous numerical predictions [11]. The FOPCPO is self-starting from noise and is stable after roughly 60 roundtrips. As predicted by Brinkmann *et al.* [10], all the pulses are linearly and positively chirped, allowing compression using standard grating-based compressors. By defining the compressor dispersion coefficients using the model given in [16], it is possible to compress the pulses below 950 fs for the idler and 3 ps for the signal. The feedback ratio given by the losses of the coupler was carefully adjusted in order to allow a stable operation with coherent output pulses.

4 Experimental results

The FOPCPO output measured at 10 µJ pump energy are summarized in Figure 5a. Using time-dispersion tuning, the FOPCPO output pulses can be widely tuned over the gain bandwidth with a tunability of 30 nm for the signal (from 780 to 810 nm), and 70 nm for the idler (from 1440 to 1510 nm), with a maximum gain obtained at 800 nm and 1450 nm and a pulse duration of 260 ps has been measured using a fast detection system (25 GHz photodiode and 33 GHz oscilloscope). The output signal energy scales linearly with the pump energy and reaches 1.4 µJ, see Figure 5b.

It is worth noting that both idler and signal pulses are relatively broadband (from 5 to 10 nm), which is a major difference with the numerical simulations as narrower signal pulses were expected. The physical reason behind this discrepancy is still being investigated. However, it appears that several regimes are actually accessible by adjusting the feedback ratio. We identified two specific regimes, one with a low feedback ratio that appears slightly narrower than the one with a high feedback ratio, as depicted in Figure 6. In addition, the highest energies were obtained with the high-feedback regime.

As discussed by Zhang *et al.* [17], it appears that the output spectrum broadens as the feedback ratio increases, before reaching an unstable regime for a critical feedback ratio. Although this phenomenon is easy to detect in numerical simulations, it is no mean feat experimentally. Because of the spectrum analyser integration time, one should track the FOPCPO output dynamic pulse by pulse, by means for example of dispersive Fourier transform, however it needs a spool of normal dispersion optical fiber at the wavelength of interest. Pulse compression is an ongoing work, as it can be a challenging task for oscillators that exhibits several dynamic behaviors.

5 Outline and prospects

We demonstrate that using highly chirped pulses in combination with PCF ends functionalization to mitigate fiber tips damage, energy scaling of the FOPCPO scheme beyond the microjoule barrier is possible. This opens the path for the development of widely tunable parametric oscillators delivering high energy levels at high-repetition rates. These features would make FOPCPOs prominent sources for stimulated coherent Raman spectroscopy

Table 1. Simulation parameters of the FOPCPO.

Element	Length (m)	α (m^{-1})	γ ($W^{-1} \cdot m^{-1}$)	β^2 ($s^2 \cdot m^{-1}$)	β^3 ($s^3 \cdot m^{-1}$)	β^4 ($s^4 \cdot m^{-1}$)	λ_{cut} (nm)
SUP-5-125	0.08	0.002	15	$2.17.10^{-27}$ @1040 nm	$6.36.10^{-41}$ @1040 nm	$-8.9.10^{-56}$ @1040 nm	
PM780	200	0.002	10	$4.31.10^{-26}$ @785 nm	$2.37.10^{-41}$ @785 nm	$-1.38.10^{-56}$ @785 nm	
Coupler		13					
Filter							980 nm shortpass filter

The gray shaded areas correspond to parameters that cannot be applied to the corresponding elements. For example, the length of the filter cannot be defined as it is not a fiber component.

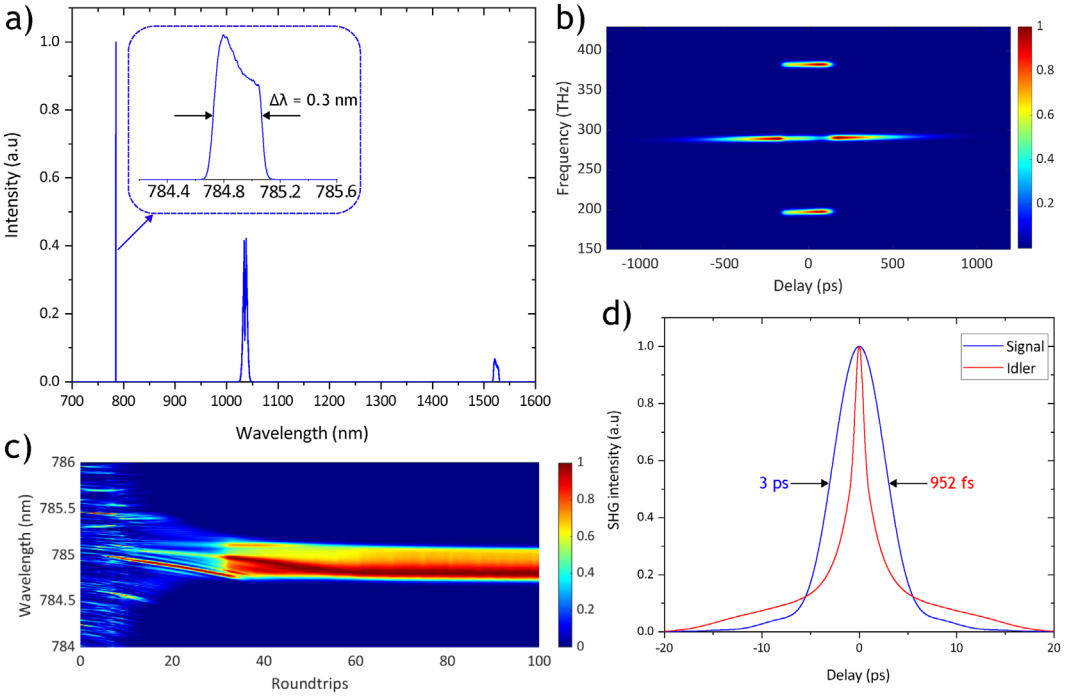

Figure 4. Numerical results. a) Output spectrum of the FOPCPO. b) Output spectrogram. c) Signal wave build-up. d) Autocorrelation traces of the dechirped signal and idler pulses.

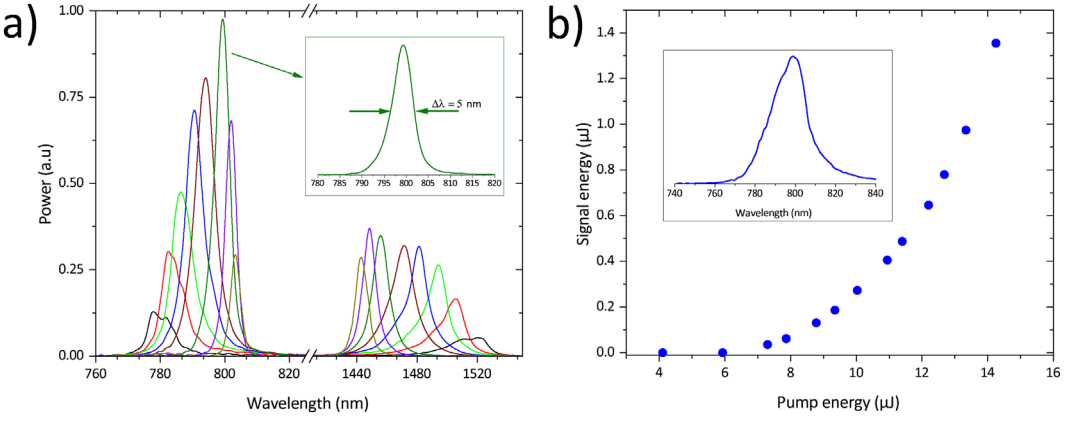

Figure 5. a) FOPCPO tunability for a pumping energy of 10 μJ. Power is normalized to the highest value obtained at 800 nm (see inset). b) FOPCPO energy scaling. Inset: Output spectrum at nominal power.

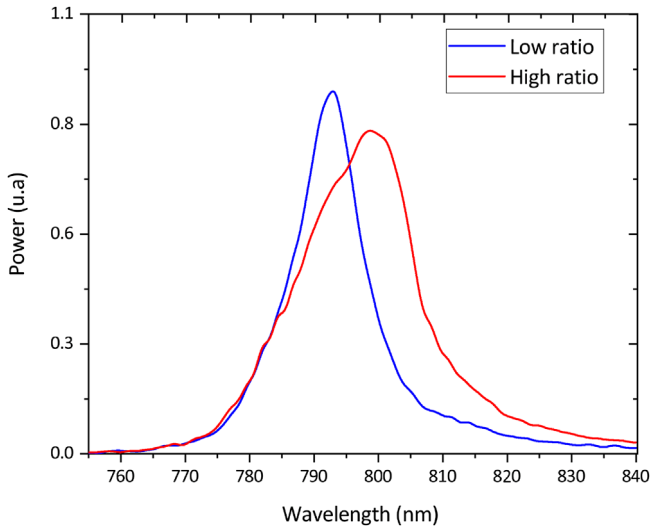

Figure 6. Impact of the feedback ratio on the output signal spectrum.

(SRS) [18], or multiphoton imaging [19]. Further experiments should now be done on pulse compression and the impact of the feedback ratio on the dynamics of the pulses. However, the chirp properties of such a system could also be used without compression in a spectral focusing based SRS setup [20, 21].

Funding

The authors acknowledge the support of the Conseil Régional de Normandie and the European Regional Development Fund, the Région Bretagne, the Département des Côtes d'Armor, Lannion-Trégor Communauté (LTC) and the Agence Nationale de la Recherche et de la Technologie (ANRT).

Conflicts of Interest

The authors declare no conflict of interests

Data availability statement

Data underlying the results presented in this paper are not publicly available at this time but may be obtained from the authors upon reasonable request.

Author contribution statement

All authors made significant contributions to this work.

References

1 Dubietis A., Matijošius A. (2023) Table-top optical parametric chirped pulse amplifiers: past and present, *Opto-Electron Adv.* **6**, 220046.

2 Hanna M., Druon F., Georges P. (2006) Fiber optical parametric chirped-pulse amplification in the femtosecond regime, *Opt. Express* **14**, 2783–2790.

3 Morin P., Dubertrand J., Beaure d'Augeres P., Quiquempois Y., Bouwmans G., Mussot A., Hugonnot E. (2018) µJ-level Raman-assisted fiber optical parametric chirped-pulse amplification, *Opt. Lett.* **43**, 4683–4686.

4 Lafargue L., Scol F., Vanvincq O., Poeydebat E., Bouwmans G., Hugonnot E. (2022) All-polarization-maintaining and high-energy fiber optical parametric chirped-pulse amplification system using a solid core photonic hybrid fiber, *Opt. Lett.* **47**, 4347–4350.

5 Fu W., Wise F.W. (2018) Normal-dispersion fiber optical parametric chirped-pulse amplification, *Opt. Lett.* **43**, 5331–5334.

6 Qin Y., Batjargal O., Cromey B., Kieu K. (2020) All-fiber high-power 1700 nm femtosecond laser based on optical parametric chirped-pulse amplification, *Opt. Express* **28**, 2317–2325.

7 Fu W., Herda R., Wise F.W. (2020) Design guidelines for normal-dispersion fiber optical parametric chirped-pulse amplifiers, *J. Opt. Soc. Am. B* **37**, 1790–1805.

8 Gottschall T., Meyer T., Schmitt M., Popp J., Limpert J., Tünnermann A. (2015) Four-wave-mixing-based optical parametric oscillator delivering energetic, tunable, chirped femtosecond pulses for non-linear biomedical applications, *Opt. Express* **23**, 23968–23977.

9 Gottschall T., Limpert J., Tünnermann A. (2017) Ultra-short pulse fiber optical parametric oscillator, *Opt. Lett.* **42**, 3423–3426.

10 Brinkmann M., Hellwig T., Fallnich C. (2017) Optical parametric chirped pulse oscillation, *Opt. Express* **25**, 12884–12895.

11 Becheker R., Touil M., Idlahcen S., Tang M., Haboucha A., Barviau B., Grisch F., Camy P., Godin T., Hideur A. (2020) High-energy normal-dispersion fiber optical parametric chirped-pulse oscillator, *Opt. Lett.* **45**, 6398–6401.

12 Zhou Y., Cheung K.K.Y., Yang S., Chui P.C., Wong K.K.Y. (2009) A time-dispersion-tuned picosecond fiber-optical parametric oscillator, *IEEE Photonics Technol. Lett.* **21**, 17, 1223–1225.

13 Balac S., Fernandez A., Mahé F., Méhats F., Texier-Picard R. (2016) The interaction picture method for solving the generalized nonlinear Schrödinger equation in optics, *ESAIM: M2AN* **50**, 4, 945–964.

14 Sørensen S.T. (2013) *Deep-blue supercontinuum light sources based on tapered photonic crystal fibers*, Technical University of Denmark.

15 Fork R.L., Brito Cruz C.H., Becker P.C., Shank C.V. (1987) Compression of optical pulses to six femtoseconds by using cubic phase compensation, *Opt. Letters* **12**, 7, 483.

16 Hugonnot E. (2019) Chirped-pulse amplification, *Techniques de l'ingénieur*, **TIP520WEB**, e6515. Available at https://doi.org/10.51257/a-v1-e6515.

17 Zhang W.Q., Sharping J.E., White R.T., Monro T.M., Shahraam Afshar V. (2010) Design and optimization of fiber optical parametric oscillators for femtosecond pulse generation, *Opt. Express* **18**, 17294–17305.

18 Kong C., Pilger C., Hachmeister H., Wei X., Cheung T.H., Lai C.S.W., Lee N.P., Tsia K.K., Wong K.K.Y., Huser T. (2020) High-contrast, fast chemical imaging by coherent Raman scattering using a self-synchronized two-colour fiber laser, *Light Sci. Appl.* **9**, 25.

19 Horton N., Wang K., Kobat D., Clark C.G., Wise F.W., Schaffer C. B., Xu C. (2013) In vivo three-photon microscopy of subcortical structures within an intact mouse brain, *Nature Photon.* **7**, 205–209.

20 Chen K., Wu T., Chen T., Wei H., Yang H., Zhou T., Li Y. (2017) Spectral focusing dual-comb coherent anti-Stokes Raman spectroscopic imaging, *Opt. Lett.* **42**, 3634–3637.

21 Qin Y., Cromey B., Batjargal O., Kieu K. (2021) All-fiber single-cavity dual-comb for coherent anti-Stokes Raman scattering spectroscopy based on spectral focusing, *Opt. Lett.* **46**, 146–149.